Mode-coupling behavior of a Lennard-Jones binary mixture upon increasing confinement

P. Gallo,* A. Attili, and M. Rovere
Dipartimento di Fisica, Università "Roma Tre," Via della Vasca Navale 84, 00146 Roma, Italy
(Received 23 December 2008; revised manuscript received 26 October 2009; published 23 December 2009)

Molecular dynamics simulations are performed on a Lennard Jones binary mixture confined in off lattice matrices of soft spheres with increasing radius. We focus on dynamics upon supercooling and in particular on testing the mode coupling theory properties of the confined mixture. Parameters of mode coupling theory in going from bulk to weak confinement, and from weak to strong confinement are extracted from simulations and analyzed. We focus on the study of the behavior of the single particle density correlators. We find that the mode coupling theory retains its validity also in the case of strong confinement, with a reduction of range of validity. The role of hopping is discussed in relation with the differences between the results obtained from the diffusion coefficients and the mode coupling theory predictions.

DOI: 10.1103/PhysRevE.80.061502 PACS number(s): 64.70.P−, 61.20.Ja, 61.20.Lc

I. INTRODUCTION

During the last years an intense debate has been developing on glass transition in confinement. This issue is of large interest in biology, geophysics, and for technological applications where confined fluids often play fundamental roles [1,2].

How the glass transition scenario transfers in going from bulk to confined phases it is a question whose answer might depend on the type of confinement [3]. Nonetheless general trends and universal features are emerging out of the many diversified kinds of confinement that have been under the scrutiny of the scientific community involved. One of the important achievements in this field has been that the mode coupling theory [4–7], MCT, of the evolution of glassy dynamics, works well also in several kinds of confinement [8–17].

The MCT is able to describe the dynamics of bulk liquids in the supercooled region on approaching a crossover temperature T_C. Above T_C ergodicity is attained through structural relaxations while below this temperature structural relaxations are frozen and only activated processes permit the exploration of the configurational space. When also hopping is frozen the system reaches the temperature of glass transition. Above T_C the relaxation mechanism of the supercooled liquid can be described as mastered by the cage effect. Nearest neighbors surround and trap the tagged particle forming a cage around it. When the cage relaxes, due to cooperative motions, the particle diffuses. The MCT describes the dynamics for the density correlator $\phi_q(t)$ introducing a retarded memory function. In the idealized version of the MCT, hopping processes are neglected and the nonlinear set of integrodifferential equations can be solved analytically to the leading order in $\epsilon=(T-T_C)/T_C$, the small parameter of the theory, deriving universal results for the behavior of the density correlator. Within these approximations T_C is the temperature of structural arrest of the ideal system. The success of this theory is due to the fact that on approaching T_C from above the predictions of the idealized version of the MCT are verified in experiments and computer simulations [47].

In many systems hopping starts to appear above and close to T_C introducing small deviations from the idealized behavior. The role of hopping, closely connected to dynamical etherogeneities [18], seems to be enhanced in confinement or in mixture with large size disparity [19–22] close and above T_C [10–13].

Depending on degree and type of confinement novel features recently emerged [23–28] in the density correlators characterizing higher order MCT transitions [29,30], analogous to what found in colloids [31–33]. Unified mean field approaches for bulk liquids, colloids and confined liquids have been also investigated [34–36].

In this framework it is important to understand if the validity of MCT is preserved in situations of strong confinement. Studies upon decreasing the free volume accessible for the liquid are therefore significative to deeply understand the role of restricted geometries [37].

Liquids confined in network of interconnected pores with a large value of porosity, as silica xerogels, can be appropriately studied with models where the confining solid is built as a disordered array of frozen microspheres [38–41]. We consider here one such a system, a liquid Lennard-Jones binary mixture, LJBM, composed of 80% of particles A and 20% of smaller particles B embedded in an off-lattice matrix of soft spheres. In the bulk phase this LJBM has been proven to show upon supercooling a dynamical behavior in agreement with the predictions of MCT [42–44]. In previous studies we tested the MCT behavior of this confined mixture for a single size of the spheres [11–13] and we compared it with an equivalent bulk [10]. The present study represents an extension of the previous work in which we study the behavior of several systems upon increasing the size of the confining spheres upon supercooling by performing MCT tests on the systems and comparing the results.

The paper is structured as follows, in the next section we describe the simulation details. In the Sec. III we analyze the static properties of the systems. In the Sec. IV we study the mean square displacement (MSD) behavior. Sections V and VI deal with the van Hove self-correlation functions and its space Fourier transform, the intermediate scattering function, respectively. The last section is devoted to conclusions.

*Author to whom correspondence should be addressed; gallop@fis.uniroma3.it

II. SIMULATION DETAILS

We report data analysis obtained from MD simulations trajectories of a Lennard-Jones 80:20 binary mixture (LJBM) defined as in Refs. [42–44]. In the following the 80% particles will be referred to as A and the 20% as B. We analyze the behavior of the binary mixture in confined states by embedding the LJBM in a disordered array of soft spheres, labeled with M in the following.

The particles interact with the potential,

$$V_{\mu\nu} = 4\epsilon_{\mu\nu}\left[\left(\frac{\sigma_{\mu\nu}}{r}\right)^{12} - \eta_{\mu\nu}\left(\frac{\sigma_{\mu\nu}}{r}\right)^{6}\right], \quad (1)$$

where $\mu\nu \in \{A,B,M\}$. The cutoff range of the interactions is given by $r_C = 2.5\sigma_{\mu\nu}$ and, in order to avoid the discontinuity at $r = r_C$, the potentials are shifted. The simulations have been performed in a cubic cell where periodic boundary conditions have been applied. In the following Lennard-Jones units are used.

The total number of A and B particles is $N = 1000$. Both types of particles have the same mass $m_A = m_B = 1$. The parameters $\sigma_{\mu\nu}$ and $\epsilon_{\mu\nu}$ of the LJBM potential ($\eta_{\mu\nu} = 1$) are given by $\sigma_{AA} = 1.0$, $\sigma_{AB} = 0.8$, $\sigma_{BB} = 0.88$, $\epsilon_{AA} = 1.0$, $\epsilon_{AB} = 1.5$, and $\epsilon_{BB} = 0.5$.

The simulation box of the confined systems contains a rigid disordered array of $N_M = 16$ soft spheres. To obtain different confining conditions the parameter σ_M of the soft sphere potential is changed while maintaining fixed the volume of the simulation box. The parameters chosen for the soft spheres interaction potential ($\eta_{M\nu} = 0$) are $\sigma_M = 1.0$, 2.0 and 3.0 and $\epsilon_M = 0.1$. The Lorentz-Berthelot mixing rules have been used to obtain the values of the parameters of interactions of the soft spheres with A and B particles. We simulated also the bulk and we will in the following refer to the bulk as the $\sigma_M = 0.0$ case. Snapshots of the simulated systems are reported in Fig. 1.

The realization of each of the confined systems is described in the following: we equilibrated at high temperature, $T = 5.0$, a bulk system done of 816 A particles and 200 B particles, using a constant volume with a selected simulation box length $L = 9.6873$. This corresponds to a number density of the bulk of $\rho = 1.1$. This value is the lowest density reported as thermodynamically stable in the bulk [45]. Then we randomly chose 16 A particles in a way that they are far apart at least σ_M (boundary condition included). The chosen particles are fixed in their positions and their potential is gradually switched to the soft spheres one until equilibration is reached. Starting from $T = 5.0$ all system are then cooled and equilibrated via a velocity rescaling procedure. For each thermodynamical point, MD simulations to evaluate statistical and dynamical properties have been performed in the microcanonical ensemble.

The confined systems were studied for temperatures ranging from $T = 5$ down to $T = 0.30$ for $\sigma_M = 0.0$, to $T = 0.35$ for $\sigma_M = 1.0$, to $T = 0.50$ for $\sigma_M = 2.0$ and to $T = 1.0$ for $\sigma_M = 3.0$. These are the lowest temperatures at which for each system we were able to equilibrate.

For each temperature investigated an equilibration time longer than the relaxation time of the system has been simulated. The total production time of the lowest temperature investigated, $T = 0.30$, was of $t_{\mathrm{run}} = 14$ millions of time steps. This value would correspond to a temperature of 35.9 K and $t_{\mathrm{run}} = 4.2$ μs for liquid Argon.

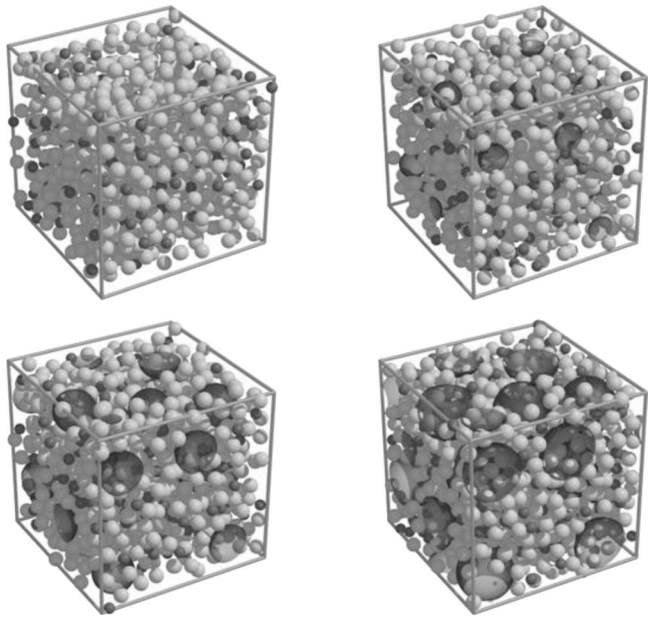

FIG. 1. Snapshots of the simulation cells for the different systems. Top left $\sigma_M = 0.0$ (bulk), top right $\sigma_M = 1.0$, bottom left $\sigma_M = 2.0$, bottom right $\sigma_M = 3.0$. Light gray spheres are A particles, dark gray small spheres are B particles. The soft spheres that form the confining system are represented by their isopotential surfaces (dark gray transparent surfaces).

We also checked that the results of the simulations are not sensitive to a specific choice of the disordered matrix by doing three different realizations of the disordered array for each size of the spheres. Our production times are always much longer than the relaxation times and therefore the correlation functions calculated for the different realizations of the systems coincide.

The behavior of the total energy calculated in the microcanonical ensemble is reported in Fig. 2 as function of the inverse temperature for systems from $\sigma_M = 0.0$ to $\sigma_M = 3.0$. The energies of the systems with bigger soft sphere size lie above those with the smallest ones. This effect is due to the term of the fluid-matrix potential energy which in fact increases with the size σ_M. From the figure we further note that upon cooling we do not observe any abrupt change in the energy. We also checked systematically during our MD runs that there was not any signature of instabilities in the thermodynamical quantities studied as function of the simulation time. In comparing the curves of Fig. 2 we note that in the system with $\sigma_M = 3.0$ the LJBM is strongly confined. In fact the lowest temperature where equilibration could be reached for the system lies in a region in which the energy is still rapidly decreasing. In this kind of region the other systems are still very liquidlike and for them the lowest reachable temperatures are in regions where a flattening of the energy curves is observed.

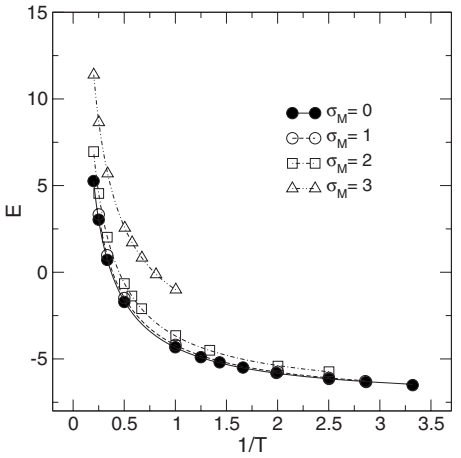

FIG. 2. Total energy per particle as function of inverse temperature for bulk (σ_M=0.0) and confined LJBM.

III. STATIC RESULTS

In the following we present and discuss the main structural properties obtained for our systems compared with the bulk case (σ_M=0.0). In Figs. 3–5 we report the radial distribution functions (RDF) $g_{\mu\nu}(r)$ (μ,ν=A,B). The results are plotted for each size σ_M at the different temperatures investigated. The RDF are vertically shifted by a quantity Δg =$(T^{-1}-1)$.

The first peak of each $g_{\mu\nu}(r)$ is approximately located at the distance r=$\sigma_{\mu\nu}$. The height of the first peaks of the RDF's of the confined systems increases by increasing the soft sphere size due to the corresponding increase of the effective density. In each system when the temperature is lowered the first neighbor peak of the $g_{AA}(r)$ and $g_{AB}(r)$ RDF becomes gradually narrower and higher, see Figs. 3 and 4. This effect is enhanced in the confined systems in comparison with the bulk and it indicates an increasing packing of the particles in the systems due to the presence of the soft spheres. The broad second neighbor peak becomes more structured at the lower temperatures and evolves in a double peak structure in the $g_{AA}(r)$ for the cases σ_M=2.0 and σ_M =3.0, in the $g_{AB}(r)$ for all σ_M. The splitting of the second peak is often observed in supercooled liquids and also corresponds to an increase of local packing of the particles [10,42–44].

From Fig. 5 it is evident that the first shell of the B particles is less defined with respect to the first nearest neighbor shell of the A particles. This is due to the interaction potential where the A-A and the A-B attractions prevail on the B-B attraction. While in the bulk at decreasing temperature the first peak of the $g_{BB}(r)$ becomes more evident, for the confined LJBM the first peak is reduced and evolves in a small shoulder at increasing size of the soft spheres. This behavior joint to the increase of the first peak of the $g_{AB}(r)$ upon cooling, see Fig. 4, suggests that the confinement induces a mixing effect at least up to the largest size investigated,

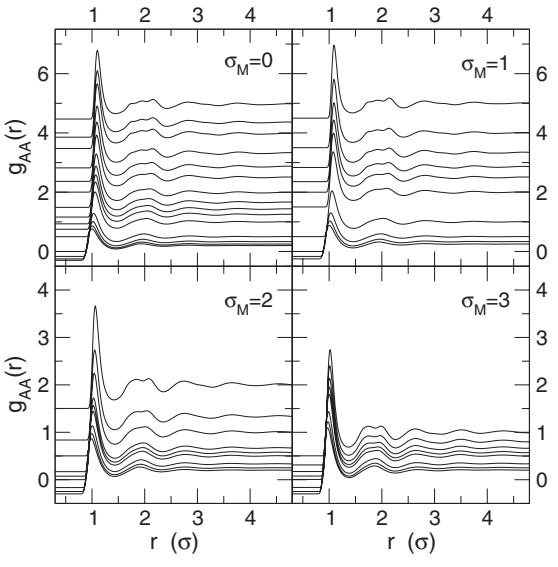

FIG. 3. Radial distribution functions $g_{AA}(r)$ for the different systems as indicated in each panel. The curves are shifted vertically by Δg=$(T^{-1}-1)$. Higher curves correspond to lower temperatures.

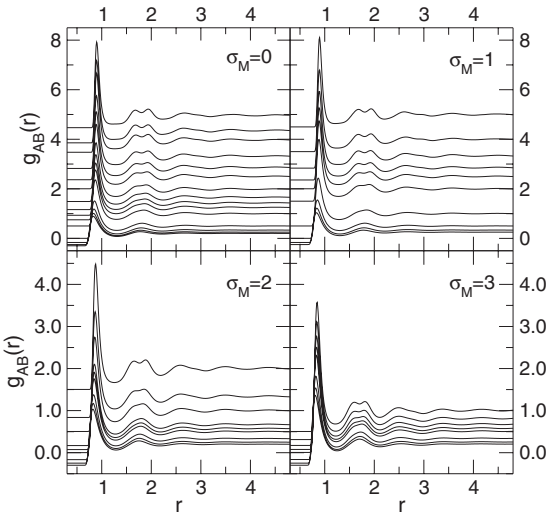

FIG. 4. Radial distribution functions $g_{AB}(r)$ reported as described in Fig. 3 for the $g_{AA}(r)$.

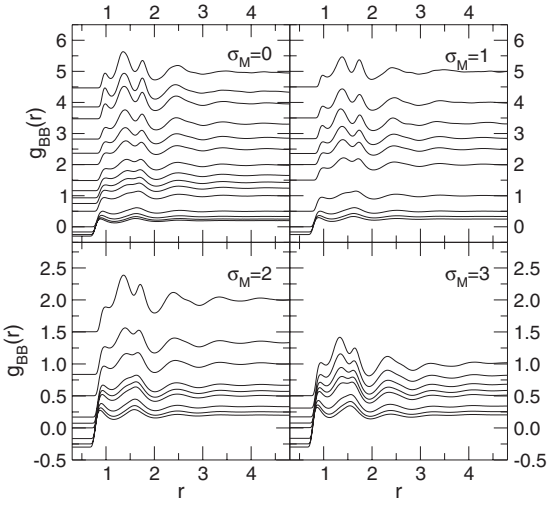

FIG. 5. Radial distribution functions $g_{BB}(r)$ reported as described in Fig. 3 for the $g_{AA}(r)$.

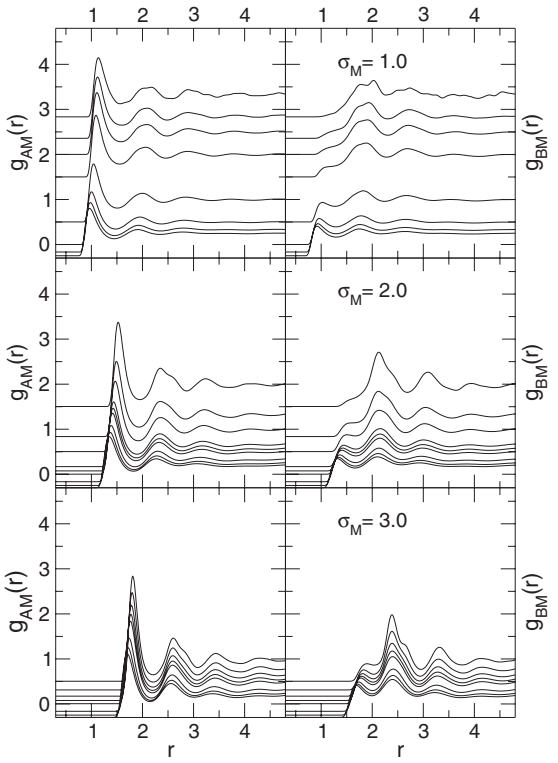

FIG. 6. Radial distribution functions between the soft spheres and the LJBM particles for each confined system and various temperatures: $g_{AM}(r)$ on the left column and $g_{BM}(r)$ on the right column. $\sigma_M=1.0$, first row; $\sigma_M=2.0$, second row; $\sigma_M=3.0$, third row. The curves are shifted vertically by $\Delta g=(T^{-1}-1)$. Higher curves correspond to lower temperatures.

$\sigma_M=3.0$. A different behavior has been observed for the case $\sigma_M=5.0$ and $L=12.6$ where the presence of the matrix increases the repulsion between the B particles with a consequent effect of demixing [12].

We consider now the $g_{\mu M}(r)$ reported in Fig. 6 where the RDF evaluated at different temperatures are displayed together for each of the three σ_M sizes. It is easy to identify the main coordination shells of the liquid particles around the confining soft spheres. The positions of the first neighbor peaks of $g_{\mu M}(r)$ are located close to $r=\sigma_{\mu M}$ but they slightly shift to lower values at increasing temperature. We note that the second peak is split at the lower temperatures.

The main peculiar feature in Fig. 6 is the behavior of the $g_{BM}(r)$. We observe for the first peak of this correlator upon supercooling not only a shift but also a consistent and gradual reduction in correspondence of an enhancement of the second shell. This effect is the signature of a depletion of B particles from the interfacial region of the confining matrix. The B particles tend to avoid the soft spheres as the temperature is lowered.

The static structure factors (SSF) $S_{\mu\nu}(Q)$ for the A and B particles are calculated via the Fourier transform of the RDF. The SSF have the usual features that these functions present in simple liquids, in particular they depend weakly on temperature. The height of the peaks and the depth of the valleys become slightly more pronounced upon lowering the temperature, while the positions of the peaks do not change. The

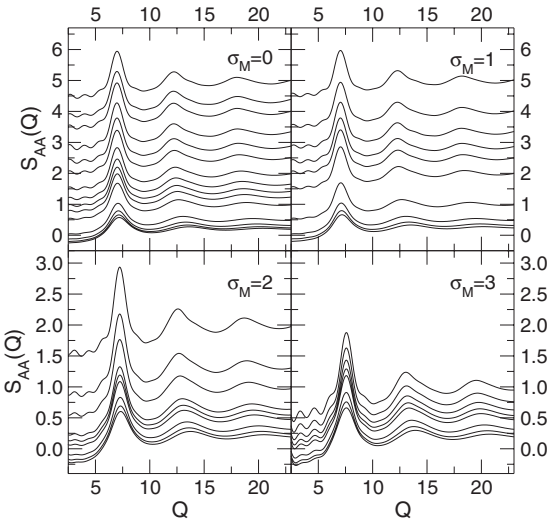

FIG. 7. Static structure factor $S_{AA}(Q)$ for each system and at different temperatures. The curves are shifted vertically by $\Delta S=(T^{-1}-1)$. Higher curves correspond to lower temperatures.

position of the first diffraction peak Q_{MAX} slightly drifts to higher values with increasing σ_M. This effect is particularly relevant for the $S_{AA}(Q)$ functions shown in Fig. 7. For the $S_{AA}(Q)$ Q_{MAX} ranges from 7.01 for $\sigma_M=0.0$ to 7.58 for $\sigma_M=3.0$. In the case of $S_{AB}(Q)$ (not shown) Q_{MAX} shifts from 7.55 to 8.00, while for the $S_{BB}(Q)$ (not shown) it goes from 5.67 to 5.90. Also this observed shift of Q_{MAX} is the signature of the increment of the close packing of the particles when the confinement becomes stronger upon increasing the size of the soft spheres.

IV. MEAN SQUARE DISPLACEMENT AND DIFFUSION COEFFICIENT

The results reported in the previous section show that there is no signature of a phase transition upon supercooling at least in the static properties. According to the MCT we expect that the dynamical properties can be strongly modified in the supercooled liquid instead.

We consider now the behavior of the MSD for decreasing temperatures. In Fig. 8 we report the MSD $\langle r_\mu^2(t)\rangle$ for each system, for A particles and for the temperatures $T=1.0$, $T=2.0$, and $T=4.0$. The B particles MSD (not shown) shows a similar trend.

In a normal liquid state the MSD is proportional to t^2 for short time, the ballistic regime, and at the onset of the diffusive, Brownian, regime becomes proportional to t. At the temperature $T=4.0$ the MSD of all the different systems show this behavior, in all cases the onset of the Brownian regime is at $t=1$. At $T=2.0$ and more significantly at $T=1.0$ a different behavior starts to appear especially for the $\sigma_M=3.0$ system. The MSD does not switch to the diffusive regime after the ballistic one, like in the high temperature range. A plateau appears at intermediate times due to the cage effect indicating that the system is approaching a glass transition. The particle rattles in the cage of the nearest neighbors and only for time long enough for the cage to relax

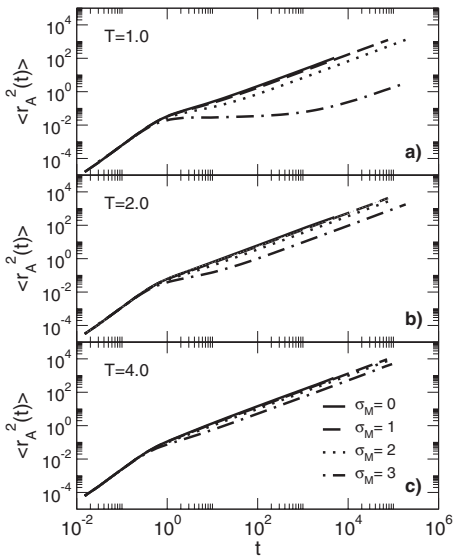

FIG. 8. Mean square displacement (MSD) of A particles $\langle r_A^2(t)\rangle$ for the different systems, $\sigma_M=0.0, 1.0, 2.0, 3.0$. (a) $T=1.0$, (b) $T=2.0$, (c) $T=4.0$.

the particle is able to escape. For the systems with $\sigma_M<3$ the plateau appears for temperatures lower than $T=1.0$.

For $\sigma_M=3.0$ and $T=1.0$ the height of the plateau is around 0.03 and from this height the cage size can be estimated to be 0.017. This value is in agreement with previous calculations on the confined LJBM [10].

By comparing the MSD of A particles and B particles (not shown) we observe that for each temperature the A particles are slower than the B. A similar behavior has been found in the bulk LJBM [42–44].

A fit of the MSD in the asymptotic Brownian regime can be performed to extract the diffusion coefficient D_μ for each specie according to the Einstein relation $\langle r_\mu^2(t)\rangle=6D_\mu t$. From the T dependence of the diffusion coefficient we can test the prediction of MCT

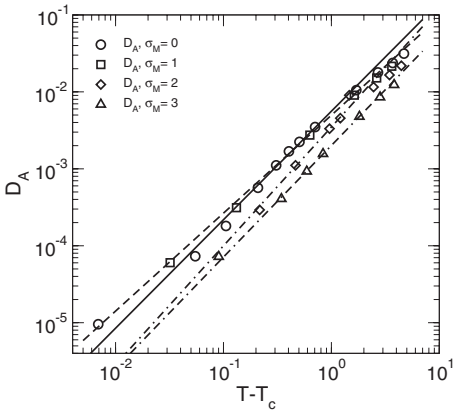

FIG. 9. Power-law fits, see Eq. (2), of the diffusion coefficients D_μ for A particles in the different systems $\sigma_M=0.0$, $\sigma_M=1.0$, $\sigma_M=2.0$, $\sigma_M=3.0$. The values of the fitting parameters are reported in Table I.

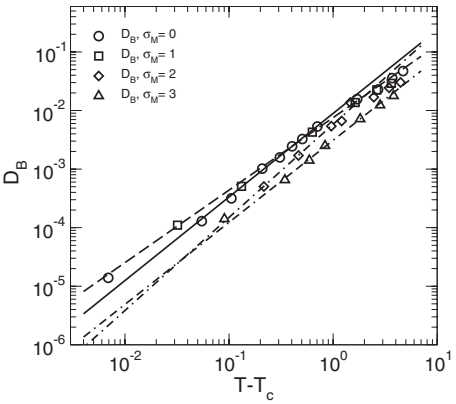

FIG. 10. Power-law fits, see Eq. (2), of the diffusion coefficients D_μ for B particles in the different systems $\sigma_M=0.0$, $\sigma_M=1.0$, $\sigma_M=2.0$, $\sigma_M=3.0$. The values of the fitting parameters are reported in Table I.

$$D_\mu \propto (T-T_C)^{\gamma_\mu}, \tag{2}$$

where T_C is the crossover temperature. It comes out that in all our cases the diffusion coefficient goes asymptotically to zero with a power law. The values of D_μ and the fitting curves are reported in Figs. 9 and 10 as function of $(T-T_C)$. MCT predicts that the crossover temperature does not depend on the different species and moreover $\gamma_A=\gamma_B$. We fitted D_A and D_B by assuming the same T_C and relaxing the condition on the exponents. The values obtained are presented in Table I. The crossover temperatures show a monotonically increasing behavior at increasing σ_M, with T_C going from the value 0.29 for $\sigma_M=0.0$ to 1.14 for $\sigma_M=3.0$. This is in agreement with what found in a film with noninteracting hard walls, where confinement is strong, and where this mixture shows an enhancement of the glass transition temperature with respect to bulk [46]. The exponents γ_A and γ_B result to be very similar for each system but they do not show any regular behavior as function of σ_M and, most importantly, the values obtained $1.2<\gamma_\mu<1.59$ are outside of the range of MCT which predicts for γ a minimum value of 1.766 [47]. As discussed in the next section this phenomenon

TABLE I. Power-laws fit parameters, for A and B particles. In the upper half of the table are reported values obtained from the analysis of diffusion constants D, while in the lower half values obtained from the analysis of relaxation times τ_α.

	$\sigma_M=0.0$	$\sigma_M=1.0$	$\sigma_M=2.0$	$\sigma_M=3.0$
		(From D)		
T_c	0.29	0.37	0.53	1.14
γ_A	1.41	1.27	1.54	1.45
γ_B	1.43	1.24	1.59	1.40
		(From τ_α)		
T_c	0.28	0.31	0.44	0.85
γ_A	2.35	2.65	3.35	4.00
γ_B	2.28	2.80	3.50	4.00

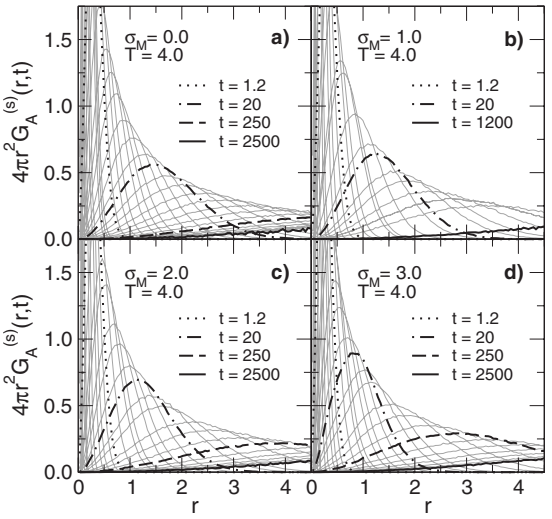

FIG. 11. SVHCF for A particles in the different systems: (a) $\sigma_M=0.0$, (b) $\sigma_M=1.0$, (c) $\sigma_M=2.0$, (d) $\sigma_M=3.0$, at $T=4.0$ for increasing time. Results for some of the times are evidenced with thicker lines.

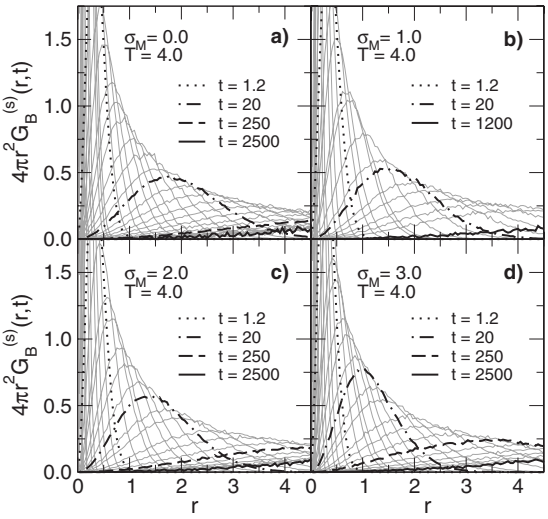

FIG. 12. SVHCF for B particles in the different systems: (a) $\sigma_M=0.0$, (b) $\sigma_M=1.0$, (c) $\sigma_M=2.0$, (d) $\sigma_M=3.0$, at $T=4.0$ for increasing time. Results for some of the times are evidenced with thicker lines.

is connected to the presence of long time hopping, which influences with D behavior.

V. VAN HOVE CORRELATION FUNCTIONS

We consider now the self-part of the van Hove correlation functions (SVHCF).

$$G_\mu^{(s)}(\mathbf{r},t)=\frac{1}{N_\mu}\left\langle\sum_{i=1}^{N_\mu}\delta(\mathbf{r}-[\mathbf{r}_i(t)-\mathbf{r}_i(0)])\right\rangle \tag{3}$$

$4\pi G_\mu^{(s)}(\mathbf{r},t)$ is the probability density to find a particle of type μ at distance $\mathbf{r}$ at time t. The SVHCF have been evaluated for different temperatures and for times that span from the ballistic to the diffusive regime of the MSD, $10^{-2}<t<10^5$ with a $t\propto 2^n$ geometric progression. The most significative results are reported in Figs. 11–15.

In Figs. 11 and 12 we show the SVHCF as function of r and different times of each system ($\sigma_M=0.0,1.0,2.0,3.0$) at $T=4.0$ for A and B particles, respectively. From the figures it is evident that at short times the SVHCF has a single peak. This peak moves to large distances as the time increases. A detailed analysis shows that the position of the peak moves approximately as $r\propto t^2$. This behavior is consistent with the ballistic regime found in the MSD at the early times. The shape of the functions is well approximated by a Gaussian. This shape is preserved also for times longer than the ballistic regime ($t\gg 1$). In this region the position of the peak r_{MAX} changes according to the diffusive regime $r_{MAX}\propto t$.

At high temperature therefore the SVHCF do not depend substantially on the confinement, apart that the dynamics for increasing value of σ_M becomes slightly slower, as already found for the MSD. As the temperature decreases differences in the behavior of the systems start to appear. In Fig. 13 the correlators of A particles are reported at $T=1.0$, the lowest temperature investigated for the system with $\sigma_M=3.0$. While the SVHCF for $\sigma_M<3$ show a behavior similar to that of the high temperatures, quite different features of the correlators appear for the $\sigma_M=3.0$ case. One of these different features is the clustering of the curves (see the bottom-right panel in Fig. 13) in the range of time $10<t<200$. This range corresponds to the plateau in the MSD and defines the β-relaxation region of the same system. Shortly after the time $t=200$ the first peak of SVHCF for the system $\sigma_M=3.0$ does not change position and decreases with time. A second peak around $r\simeq 1$ starts to appear and becomes more pronounced as the time increases. The height of this second peak becomes comparable with the first one for times long enough, $t>10^4$. A third peak also appears around $r\simeq 2$ at long times. The presence of multiple peaks in the correlation functions is connected to hopping phenomena taking place upon supercooling. The positions of these two hopping peaks

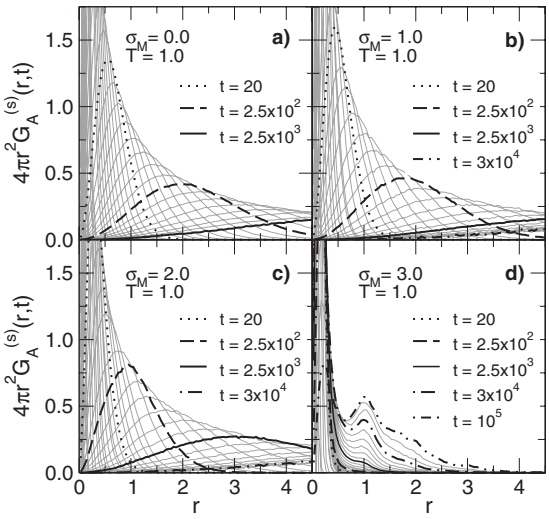

FIG. 13. SVHCF for A particles in the different systems: (a) $\sigma_M=0.0$, (b) $\sigma_M=1.0$, (c) $\sigma_M=2.0$, (d) $\sigma_M=3.0$, at $T=1.0$ for increasing time. Results for some of the times are evidenced with thicker lines.

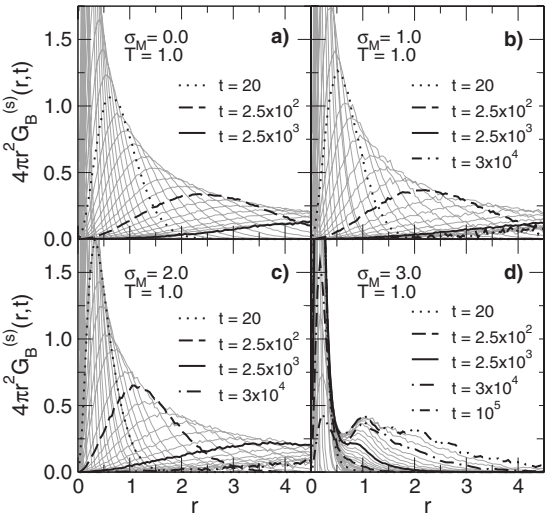

FIG. 14. SVHCF for B particles in the different systems: (a) $\sigma_M=0.0$, (b) $\sigma_M=1.0$, (c) $\sigma_M=2.0$, (d) $\sigma_M=3.0$, at $T=1.0$ for increasing time. Results for some of the times are evidenced with thicker lines.

correspond to the positions of the first two peaks of the $g_{AA}(r)$ reported in Fig. 3. In fact the single particle below a certain temperature starts to diffuse through hopping processes and moves to energetically favored positions corresponding to the peaks of the static pair correlation function.

The behavior of the SVHCF of B particles, shown in Fig. 14 at the same temperature $T=1.0$, is similar to that found for A particles. The positions of the peaks are slightly shifted at higher distances with respect to those of the SVHCF of A particles due to the higher mobility of the B specie. In the case $\sigma_M=3.0$ a multiple peak structure appears for long time as for A particles, but now the secondary peaks are broader with respect to the results reported in Fig. 13. This indicates

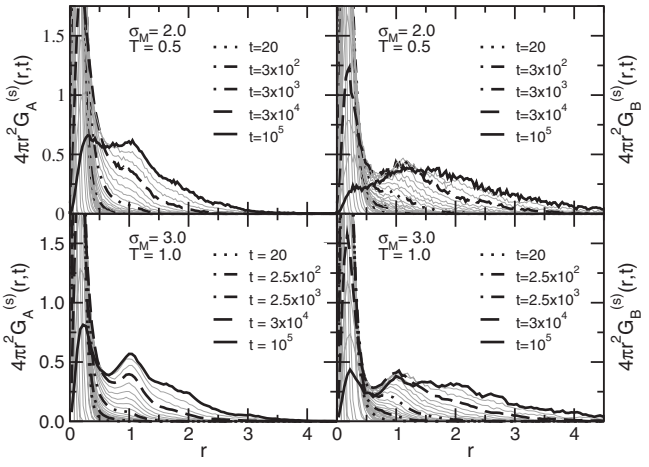

FIG. 15. SVHCF for A and B particles and for increasing time in two different systems $\sigma_M=2.0$ and $\sigma_M=3.0$ at $T=0.5$ and $T=1.0$, respectively. These two temperatures are the lowest temperatures to which the systems were equilibrated and they correspond to similar values of the small parameter of MCT, $\epsilon=0.14$ and 0.17, respectively. Results for some of the times are evidenced with thicker lines.

a more significative presence of hopping effects for B particles.

A behavior of the SVHCF similar to that of the system with $\sigma_M=3.0$ for $T=1$ can be found for the other systems at the lowest temperatures simulated. In Fig. 15 we compare the behavior of the SVHCF for $\sigma_M=2.0$ and $\sigma_M=3.0$ at the lowest temperatures investigated, namely, $T=0.5$ and $T=1$, respectively. These temperatures can be compared in the two systems as they correspond to similar small parameters, $\epsilon=(T-T_C)/T_C$ of the theory (see next section for the determination of T_C). Both SVHCF of A and B particles are reported for increasing times. We observe that hopping phenomena for smaller B particles do not seem to be very different between the two systems, and they are also very similar in the bulk [10]. Hopping phenomena of A particles appear more sensitive to confinement. They are in fact practically absent in the bulk [43]. In confinement for $\sigma_M=2.0$ they appear only for the longest times while they are more marked for the case $\sigma_M=3.0$, the strongest confinement investigated. This result indicates that hopping processes may intervene crucially in confinement possibly hiding the MCT behavior while still present. In fact we note that, especially for A particles and especially for the strongest confinement, when hopping starts to appear the first peak, related to structural arrangements, is still in the region of the plateau of the MSD. As we will see in Sec. VI B this will introduce small deviations from MCT also in the τ_α behavior for the case $\sigma_M=3.0$.

VI. SELF-INTERMEDIATE SCATTERING FUNCTIONS

Structural relaxation and slowing down of the dynamics close to the crossover temperature T_C can be conveniently characterized by analyzing the self-intermediate scattering function (SISF),

$$F_\mu^{(s)}(\mathbf{Q},t)=\frac{1}{N_\mu}\left\langle \sum_{i=1}^{N_\mu}\exp(-i\mathbf{Q}\cdot[\mathbf{r}_i(t)-\mathbf{r}_i(0)])\right\rangle. \quad (4)$$

The time dependence of these correlation functions is analyzed for the wave vector $Q=Q_{MAX}$ corresponding to the position of the main peak of the static structure factors $S_{AA}(Q)$ and $S_{BB}(Q)$. As discussed above the positions of the main diffraction peak are weakly dependent on the temperature. Thus we fix the values of Q_{MAX} to the average positions found at the lowest simulated temperature. The wave vector values used are: $Q_{MAX,A}=7.01,7.05,7.24,7.58$ and $Q_{MAX,B}=5.67,5.69,5.74,5.90$ for increasing σ_M values.

In Fig. 16 results are reported of the SISF calculated at three temperatures $T=1.0,2.0,4.0$ for the different confinements. At high temperature ($T=4.0$) each correlator for both A and B particles shows a quadratic dependence on time for $t<0.1$ in the ballistic regime. For $t\gg0.1$ the SISF decay quickly to zero with an exponential relaxation behavior. A slight departure from the exponential decay is however observed for the confined $\sigma_M=3.0$ system. This effect is more enhanced at $T=2.0$, where a small shoulder appears for intermediate time ($1<t<10$).

At the lowest temperature simulated for the system $\sigma_M=3.0$, $T=1.0$, the shoulder becomes more pronounced and

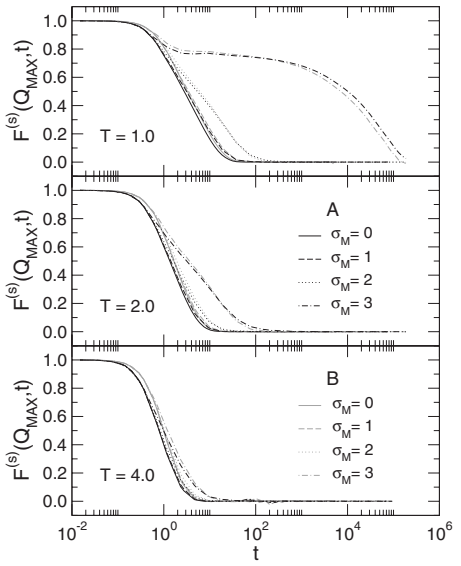

FIG. 16. SISF $F_{\mu}^{(s)}(Q_{MAX},t)$ for A (black lines) and B (gray lines) particles confined in the different system as indicated for $T=4.0$, $T=2.0$, and $T=1.0$.

spans over a greater time range $1<t<10^3$. The SISF exhibits the two step relaxation phenomenon predicted by MCT. The intermediate region where the SISF decays very slowly is described as the β relaxation regime and corresponds to the plateau region of the MSD.

The final decay to zero of the SISF corresponds to the α relaxation region. We now address our analysis to this important relaxation process in all systems.

A. α relaxation

According to the MCT we can fit the behavior of the SISF in the α relaxation region with the Kohlrausch-Williams-Watts (KWW) stretched exponential

$$f_{\mu}(t) = f_{\mu}^{c} \exp[-(t/\tau_{\alpha,\mu})^{\beta_{\mu}}], \tag{5}$$

where the exponent β_{μ} must be in the range $0<\beta_{\mu}<1$, $\tau_{\alpha,\mu}$ is the relaxation time and f_{μ}^{c} is the nonergodicity parameter. In Fig. 17 and 18 fits to the Eq. (5) of the SISF are reported for each different value of σ_M for A and B particles.

The range of temperatures investigated in this analysis is different for each system. In particular for $\sigma_M=0.0$ (the bulk) the range is: $0.30\leq T\leq 0.60$, for $\sigma_M=1.0$: $0.35\leq T\leq 1.0$, for $\sigma_M=2.0$: $0.5\leq T\leq 1.5$, for $\sigma_M=3.0$: $1.0\leq T\leq 3.0$. From the figures it is evident that the low temperature curves fit very well the KWW functions for all systems.

We found that the β_{μ} exponents depend on the temperature slowly decreasing as temperature is lowered. The values obtained for the fitted curves are in the range $0.57<\beta<0.95$ and slightly decreasing with increasing σ_M.

The non ergodicity parameter $f_{Q,\mu}^{c}$ shows only a weakly increasing behavior as function of decreasing temperature with a very slight increase with increasing σ_M. We found $0.64\leq f_{Q}^{c}\leq 0.76$ for the bulk $\sigma_M=0.0$ system, $0.7\leq f_{Q}^{c}\leq 0.77$ for the $\sigma_M=1.0$ system, $0.7\leq f_{Q}^{c}\leq 0.78$ for the $\sigma_M=2.0$ system and $0.71\leq f_{Q}^{c}\leq 0.78$ for the $\sigma_M=3.0$ system.

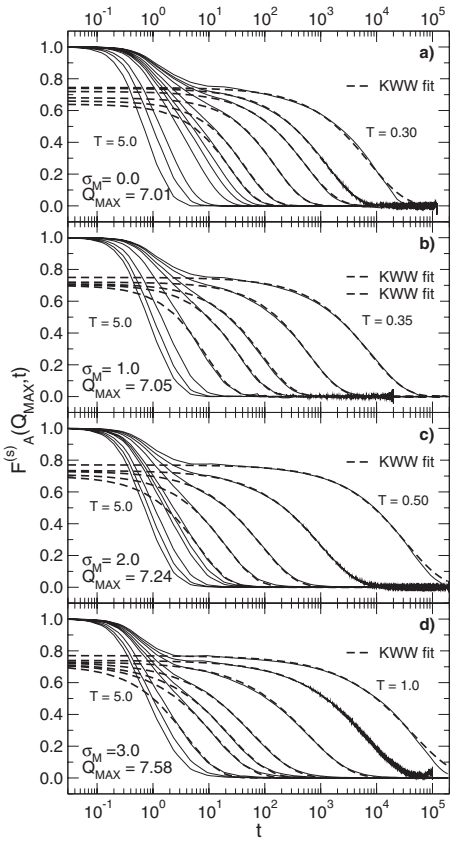

FIG. 17. SISF $F_{\mu}^{(s)}(Q_{MAX},t)$ for A particles for different temperatures and values of σ_M. From above: (a) $\sigma_M=0.0$, (b) $\sigma_M=1.0$, (c) $\sigma_M=2.0$, (d) $\sigma_M=3.0$. The dashed lines are fits to the KWW functions, see Eq. (5).

The most relevant quantity to investigate in order to define the MCT crossover temperature is the relaxation time and its dependence on the temperature. In Fig. 19 and 20 the values of $\tau_{\alpha,A}$ and $\tau_{\alpha,B}$ are reported on a log-log plots as a function of $\epsilon=(T-T_C)/T_C$. The relaxation times increase dramatically up to four orders of magnitude as the temperature is lowered. We note that the relaxation times of strongly confined systems are larger than those found for systems with smaller σ_M, this indicates the slowing down of the dynamics upon increasing the confinement. In agreement with MCT predictions there are not significative differences between the values of τ_{α} for A and B particles. The relaxation times behavior is fitted in Fig. 19 and 20 with the MCT prediction

$$\tau_{\alpha,\mu}^{-1} \propto (T-T_C)^{\gamma_{\mu}}. \tag{6}$$

We expect to find an universal crossover temperature T_C and exponents γ_{μ}. In the fitting procedure we assume the same T_C for A and B particles while the exponent can be different. The values obtained from the fitting procedure are reported in Table I and compared with the parameters obtained from the fit of the diffusion coefficients, Eq. (2).

The crossover temperature shows a monotonically increasing behavior with the confining parameter σ_M, $\gamma_A\sim\gamma_B$ and both the exponents increase with increasing σ_M. Moreover their value is in the range predicted by MCT γ

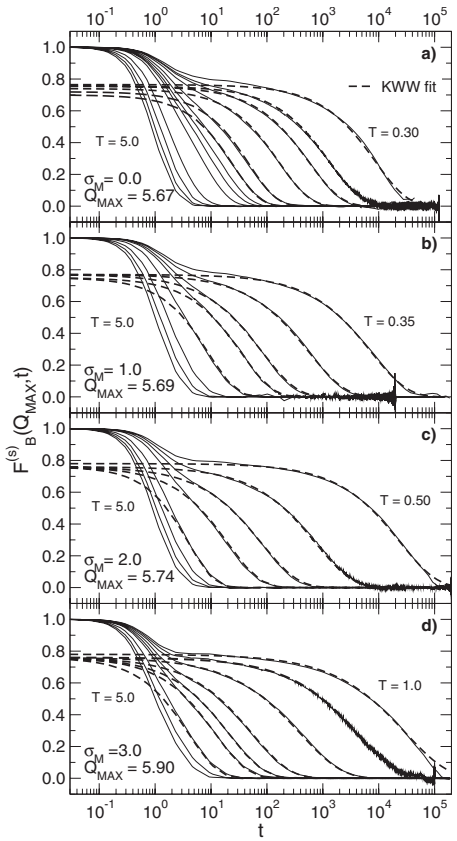

FIG. 18. SISF $F_{\mu}^{(s)}(Q_{MAX},t)$ for B particles for different temperatures and values of σ_M. From above: (a) σ_M=0.0, (b) σ_M=1.0, (c) σ_M=2.0, (d) σ_M=3.0. The dashed lines are fits to the KWW functions, see Eq. (5).

>1.766. The power-law behavior predicted by MCT, Eqs. (2) and (6) are valid in a range defined as $\epsilon=(T-T_C)/T_C$. From the figures we can note that the range of validity of MCT for the relaxation time starts for all systems at $\epsilon\sim 1$, that is $T=2T_C$. The slope of the straight line increases upon increasing soft spheres size leading to a reduction of range in

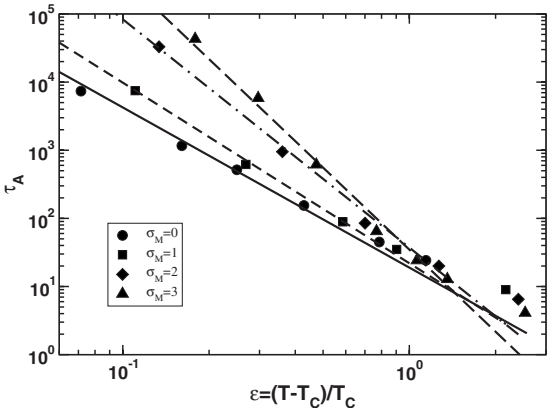

FIG. 19. Power-law fits of the relaxation time $\tau_{\alpha,\mu}^{-1}$ as a function of ϵ, for A particles for each system (σ_M=0.0,1.0,2.0,3.0). The relaxation times are obtained from KWW fits to the α regime (see Figs. 17 and 18). Parameters of the fit, T_c and exponent γ are reported in Table I.

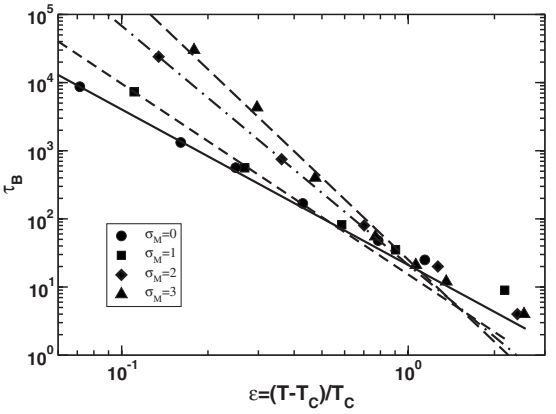

FIG. 20. Power-law fits of the relaxation time $\tau_{\alpha,\mu}^{-1}$ as a function of ϵ, for B particles for each system (σ_M=0.0,1.0,2.0,3.0). The relaxation times are obtained from KWW fits to the α regime (see Figs. 17 and 18). Parameters of the fit, T_c and exponent γ are reported in Table I.

ϵ when comparing similar relaxation times as a function of the growing soft sphere size. This leads to a 20% reduction for the case σ_M=3.0 in correspondence to the lowest temperatures to which we were able to equilibrate each system. This temperature marks for each system the crossover to a regime where hopping dominates.

The crossover temperatures obtained by fitting the $\tau_{\alpha,\mu}$ are lower than the equivalent T_C derived from the fits to the power law of D and this difference is more striking upon increasing soft spheres radii, framing in the picture of a more severe hopping that influences more markedly the D behavior for the systems with stronger confinement. We note moreover that the crossover temperatures obtained from the MSD analysis are slightly higher than the lowest temperature simulated in each confined system. Hopping coexists with structural relaxations for the lowest temperatures investigated and masks MCT behavior at long times. Also the discrepancies between the parameters γ derived from the two power-law behaviors can be attributed to the presence of hopping that causes the diffusion coefficient not to be inversely proportional to the relaxation time [48]. This has already been observed in bulk LJBM [42–44].

In Figs. 21 and 22 we report the power-law fits of the inverse of diffusion coefficients and of the relaxation times for A particles versus $1/T$. The behavior of these quantities for B particles is similar (not shown). The effect of hopping is evident from the plots. In fact we see from the figures that deviation from power-law behavior is evident only for D at low temperatures. This is due to the fact that hopping intervenes only for the lowest temperatures and on time scales longer than τ_α, causing D to switch to an Arrhenius behavior.

B. TTSP test

MCT predicts a time-temperature superposition principle (TTSP) in the asymptotic limit of $T\rightarrow T_C$. The TTSP states that the shape of the correlator curves in the late β relaxation and early α relaxation time regimes does not depend on temperature. So the intermediate scattering functions behave as

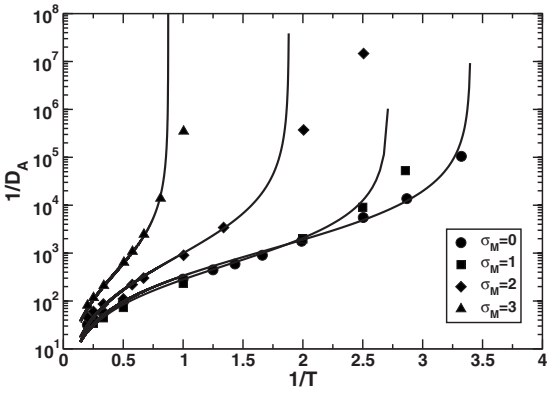

FIG. 21. Power-law fits of the inverse of the diffusion coefficients for A particles shown for all systems versus $1/T$ to better show the deviation from the power-law behavior at low temperatures.

$$F^{(s)}(Q,t) = \hat{\phi}_Q[t/\tau_\alpha(T)], \tag{7}$$

where τ_α is a time scale associated to the α-relaxation decay of the correlation function and $\hat{\phi}_Q$ is a master function. The master function $\hat{\phi}(t)$, according to MCT, has in the β-relaxation regime the functional form of the von Schweidler (VS) law,

$$\hat{\phi}(t) = f_Q^c - h_Q(t/\tau_\alpha)^b. \tag{8}$$

where f_Q^c is the non ergodicity parameter, h_Q is the amplitude factor and b is the VS exponent.

We used in the scaling of the SISF the $\tau_{\alpha,\mu}(T)$ obtained via the KWW fits of the previous subsection. In Figs. 23 and 24 we report for A and B particles respectively the SISF at $Q=Q_{MAX}$ plotted as function of $t/\tau_{\alpha,\mu}(T)$ for each system. The SISF are evaluated in the ranges of temperatures $0.30 \leq T \leq 0.60$ for $\sigma_M=0.0$, $0.35 \leq T \leq 1.0$ for $\sigma_M=1.0$, $0.5 \leq T \leq 1.5$ for $\sigma_M=2.0$, $1.0 \leq T \leq 3.0$ for $\sigma_M=3.0$. In the figures are included the best fit to the VS law, Eq. (8).

From the figures it is evident that in the long time scale of the α-relaxation regime the rescaled curves fall on top of each other defining a master curve $\hat{\phi}(t)$ with the expected stretched exponential form. The TTSP test is verified in the α regime. The TTSP holds also in the β relaxation region, where the master function can be fitted to the VS law. The parameters obtained from the VS fit are reported in Table II.

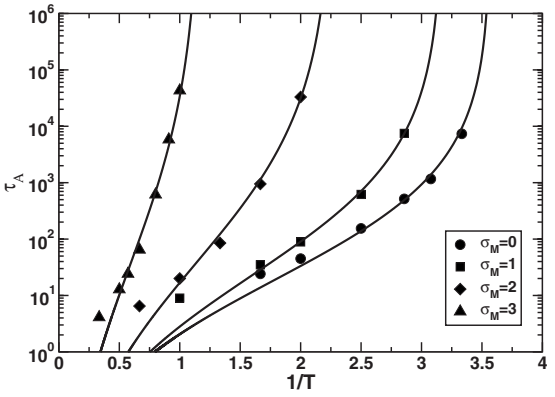

FIG. 22. Power-law fits of the relaxation time for A particles shown for all systems versus $1/T$ to better show the agreement with MCT at low temperatures.

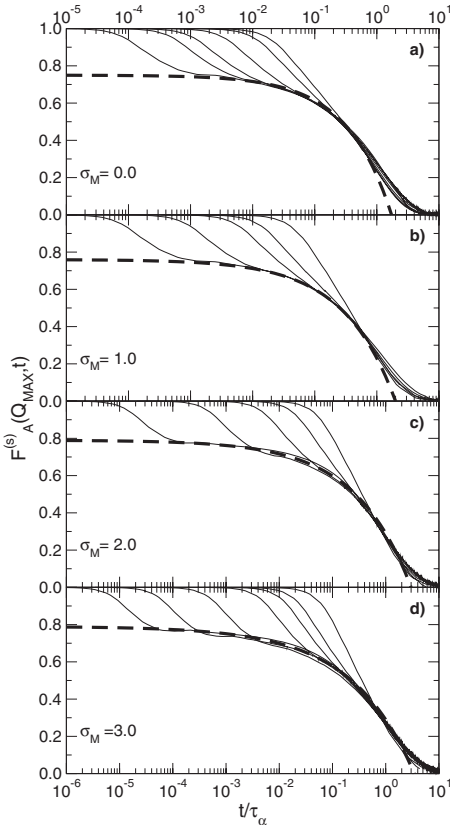

FIG. 23. Self-part of the SISF for the A particles, $F_A^{(s)}(Q,t)$, evaluated at $Q=Q_{\mathrm{MAX}}$ for each system ($\sigma_M=0.0, 1.0, 2.0, 3.0$) and different temperatures, scaled by τ_α obtained from a Kohlrausch-Williams-Watts (KWW) fit, see Fig. 17; the dashed curve is the fit to the VS law, Eq. (8). In (a) are presented $\sigma_M=0.0$ (bulk) correlators for temperatures $0.3 \leq T \leq 0.6$; (b) $\sigma_M=1.0$ correlators for temperatures $0.35 \leq T \leq 1.0$; (c) $\sigma_M=2.0$ correlators for temperatures $0.5 \leq T \leq 1.5$; (d) $\sigma_M=3.0$ correlators for temperatures $1.0 \leq T \leq 3.0$.

Starting from one parameter extracted from MD data we can calculate all the relevant MCT parameters through the relations

$$\gamma_\mu = \frac{1}{2a_\mu} + \frac{1}{2b_\mu}, \tag{9}$$

$$\lambda = \frac{\Gamma^2(1-a)}{\Gamma(1-2a)} = \frac{\Gamma^2(1+b)}{\Gamma(1+2b)}, \tag{10}$$

where Γ is the Euler Γ function, the a is related to the decay of the correlation functions toward the plateau and the exponent parameter λ characterizes the system. The parameters must be in the ranges $1/2 < \lambda < 1$, $0 < a < 0.395$, and $0 < b < 1$ [4].

Since we extracted from our analysis both γ from the τ_α and b from the VS, we calculated all the other parameters from each one of these two and compared the resulting sets.

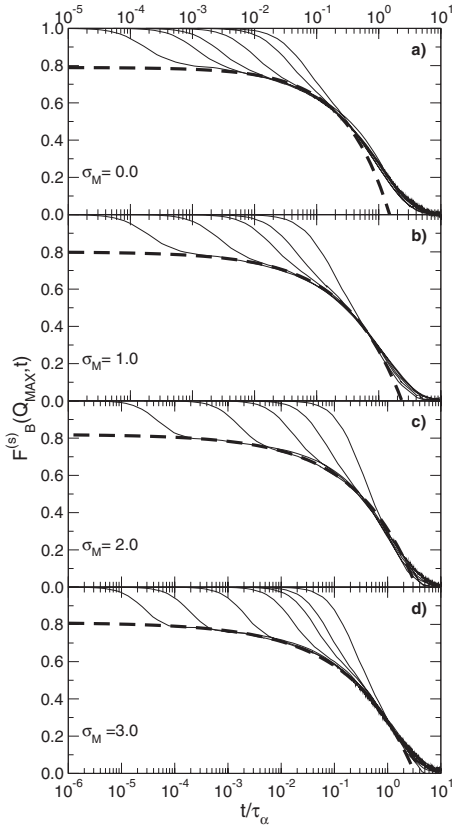

FIG. 24. Self-part of the SISF for the B particles, $F_B^{(s)}(Q,t)$, evaluated at $Q=Q_{\mathrm{MAX}}$ for each system ($\sigma_M=0.0,1.0,2.0,3.0$) and different temperatures, scaled by τ_α obtained from a Kohlrausch-Williams-Watts fit, see Fig. 18; the dashed curve is the fit to the VS law, Eq. (8). In (a) are presented $\sigma_M=0.0$ (bulk) correlators for temperatures $0.3\leq T\leq 0.6$; (b) $\sigma_M=1.0$ correlators for temperatures $0.35\leq T\leq 1.0$; (c) $\sigma_M=2.0$ correlators for temperatures $0.5\leq T\leq 1.5$; (d) $\sigma_M=3.0$ correlators for temperatures $1.0\leq T\leq 3.0$.

The values obtained are reported in Table III.

We remind that exponents γ obtained from diffusion coefficients cannot be used for this test since they are out of MCT range and therefore bring to nonconsistent b, a, and λ values. This failure is related to the strong presence of hopping processes in our systems for low temperatures and long times.

TABLE II. Von Schweider fit parameters for A and B particles of each system.

	$\sigma_M=0.0$	$\sigma_M=1.0$	$\sigma_M=2.0$	$\sigma_M=3.0$
$f_{q,A}^c$	0.75	0.76	0.79	0.79
$f_{q,B}^c$	0.79	0.80	0.82	0.82
$h_{q,A}$	0.54	0.53	0.50	0.50
$h_{q,B}$	0.62	0.53	0.51	0.53
b_A	0.60	0.52	0.42	0.37
b_B	0.60	0.48	0.38	0.36

We look at the trends of the parameters as function of the increasing size σ_M. We note that all values are similar for A and B particles, the exponents a and b decrease and the exponent parameter λ increases. It is important to stress that the two sets of parameters obtained independently from λ and from b are in very good agreement as expected for consistency with MCT equations except for $\sigma_M=3.0$ where especially in the case of γ the difference between the two sets appears more consistent. As we have seen that hopping is more significative for the stronger confinement as it starts at higher temperatures and most importantly on shorter time scales compared to the other systems investigated, therefore some deviation from MCT might start to be visible also in the τ_α values.

C. Wave-vector analysis

In Figs. 25 and 26 are reported the SISF for A and B particles respectively, evaluated at several values of the wave vector in the interval $2.5\leq Q\leq 15.0$. This is the region where the two first peaks of the $S_{AA}(Q)$ and $S_{BB}(Q)$ appear. The temperatures considered are $T=0.30,0.35,0.5,1.0$ for the systems $\sigma_M=0.0,1.0,2.0,3.0$, respectively. These temperatures correspond to similar small parameters of MCT.

TABLE III. Parameters of MCT for bulk and confined mixtures, A and B particles. In the top half of the table the values are calculated with Eqs. (9) and (10) from the b values obtained from the VS fit, see Eq. (8). In the bottom half the values are calculated with Eqs. (9) and (10) from the γ values obtained from the power-law (PL) fit of the relaxation times to the Eq. (6).

	$\sigma_M=0.0$		$\sigma_M=1.0$		$\sigma_M=2.0$		$\sigma_M=3.0$	
	A	B	A	B	A	B	A	B
b_{VS}	0.60	0.60	0.52	0.48	0.42	0.38	0.37	0.36
a_b	0.31	0.31	0.29	0.28	0.26	0.24	0.24	0.23
γ_b	2.42	2.42	2.67	2.83	3.12	3.37	3.43	3.53
λ_b	0.72	0.72	0.77	0.80	0.83	0.86	0.86	0.87
γ_{PL}	2.35	2.28	2.65	2.80	3.35	3.50	4.00	4.00
a	0.32	0.32	0.29	0.28	0.24	0.24	0.21	0.21
b	0.62	0.65	0.52	0.49	0.38	0.36	0.30	0.30
λ_a	0.71	0.72	0.77	0.79	0.85	0.86	0.90	0.90

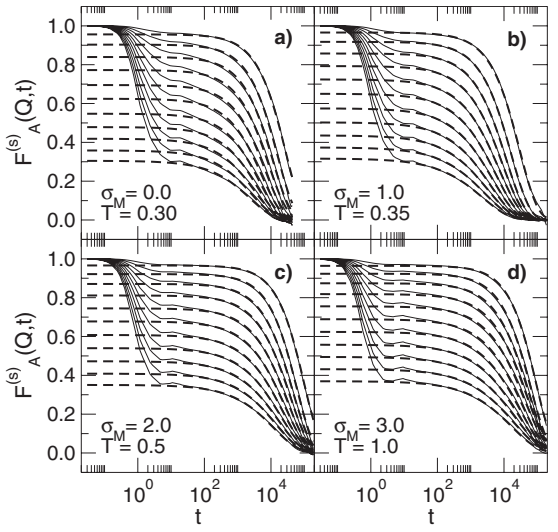

FIG. 25. SISF for the A particles, $F^s_A(q,t)$ for different wave vector values, $2.5 \leq q \leq 15$. Dashed lines are KWW fit to stretched exponential. (a) Panel: $\sigma_M=0.0$ (bulk) at $T=0.30$; (b) panel: $\sigma_M=1.0$ (bulk) at $T=0.35$; (c) panel: $\sigma_M=2.0$ at $T=0.5$; (d) panel: $\sigma_M=3.0$ at $T=1.0$. The temperature of each system corresponds to similar small parameters of MCT.

In the same figures we show the KWW best fits (dashed lines) for each SISF. The fitting parameters of the KWW curves, the relaxation time τ_α, the stretching exponent β and the nonergodicity parameter f^c_Q are reported in Fig. 27. The relaxation times show a decreasing trend with increasing wave vector Q. The values for $\sigma_M=0.0$ and 1.0 are very similar. The slope of the curves for all systems changes above $Q=5$ indicating a crossover from diffusive (low Q) to ballistic regime (large Q).

The nonergodicity parameter shows a monotonic decreasing trend. The curves for the different systems are very similar and almost coincide for B particles. The stretching parameter $\beta(Q)$ shows a slowly decreasing trend. The asymptotic behavior expected for $\beta(Q\to\infty)$ is b, the von Schweidler exponent. We see that for $\sigma_M=0.0$ and $\sigma_M=1.0$ the asymptotic values appear to converge on the same values obtained from the VS b values. For $\sigma_M=2.0$ and $\sigma_M=3.0$ the asymptotic values are higher than that calculated from the VS b values, also this inconsistency can be ascribed to the presence of hopping.

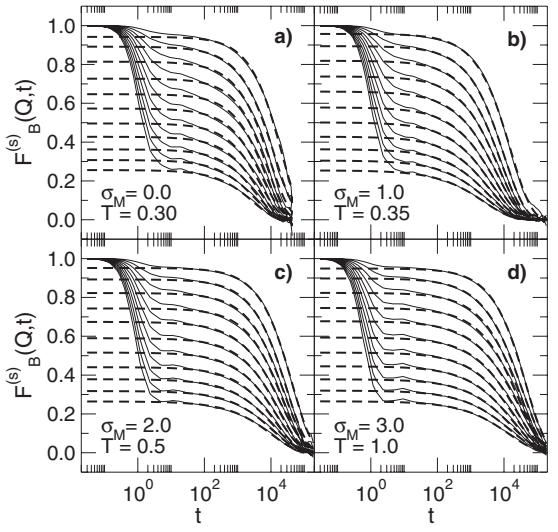

FIG. 26. SISF for the B particles, $F^s_B(q,t)$ for different wave vector values, $2.5 \leq q \leq 15$. Dashed lines are KWW fit to stretched exponential. (a) Panel: $\sigma_M=0.0$ (bulk) at $T=0.30$; (b) panel: $\sigma_M=1.0$ (bulk) at $T=0.35$; (c) panel: $\sigma_M=2.0$ at $T=0.5$; (d) panel: $\sigma_M=3.0$ at $T=1.0$. The temperatures correspond to similar small parameters of MCT.

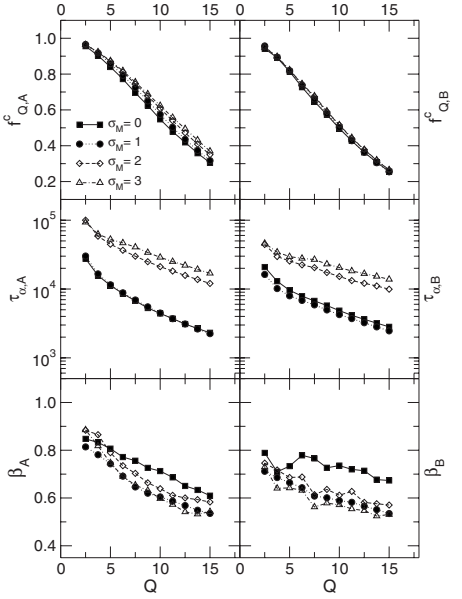

FIG. 27. Wave-vector analysis for the fitting parameter of KWW curves (shown in Figs. 25 and 26). First row of panel: Nonergodicity parameters f_q; second row: relaxation time τ_α; third row: stretching parameter β. The two columns of panels correspond to different species of particles. The analysis is carried out for each system: $\sigma_M=0.0$ at $T=0.30$, $\sigma_M=1.0$ at $T=0.35$, $\sigma_M=2.0$ at $T=0.5$, $\sigma_M=3.0$ at $T=1.0$. The temperatures correspond to similar small parameters of MCT.

VII. CONCLUSIONS

We reported results from MD simulation of a bulk LJBM and the same mixture embedded in off lattice matrices of soft spheres. We simulated four systems that differ in the size σ_M of the sixteen confining soft spheres ranging from $\sigma_M=0.0$ (bulk) to $\sigma_M=3.0$. All the systems contain 1000 LJ particles and the box length is fixed for all systems to $L=9.6873$.

The density of the bulk corresponds to the lowest stable density for the LJBM. By increasing the σ_M values the system experiences an increasing effect of confinement. For $\sigma_M=3.0$ the confinement results to be extremely strong as evident from the energy behavior.

The consistent increment of packing upon increasing the soft spheres radius induces a mixing effect especially for the highest σ_M. In spite of this the $g_{AA}(r)$, $g_{BB}(r)$ and $g_{AB}(r)$ appear all very similar to the bulk.

Analogous to what found for a confined LJBM with $\sigma_M=5.0$ and $L=12.6$ previously studied [10–13], B particles tend to avoid the soft spheres upon supercooling for all σ_M

values. Also this system specific behavior does not appear to interfere with MCT.

The onset temperature of the plateau characteristic of supercooled liquids on the MSD depends on σ_M and appears at higher temperatures for the larger σ_M. The shape the MSD and the SISF is in agreement with MCT predictions. In particular all the SISF could be fitted with the KWW function. The β exponents depend weakly on T and slightly decrease with decreasing temperature and increasing σ_M. Power-law fit τ_α values extracted from SISF show that T_C increases for increasing packing ranging from 0.28 to 0.85. The values of the exponents γ are similar for A and B particles and in the range predicted by MCT and increase upon increasing σ_M. We observe a progressive reduction of the range of validity of MCT that is reduced of 20% for $\sigma_M=3.0$.

We find discrepancies in the parameters extracted from the power-law fit to D values. The T_C values obtained from D, are systematically higher with respect to the ones extracted from the τ_α. Moreover the γ values obtained from D are outside MCT predicted range. The reason of the observed discrepancies between the two sets of γ is the presence of long time hopping in the SVHCF for all systems. Hopping intervenes to mask MCT behavior for the parameters extracted from D, as also found in the bulk [43].

Importantly the Von Schweidler law holds for all systems. VS parameters can be extracted and together with the γ extracted from the τ_α allow to determine independently the rest of the MCT exponents. The two independent determinations show similar results confirming the MCT behavior of the confined mixture. It is important to stress that MCT behavior is still present also for extremely strong confinement although some deviations can be seen in the γ values calculated from MCT parameter equations and in the asymptotic value of $\beta(Q)$.

These findings are of interest for all the cases where the microscopic behavior of supercooled confined liquids is relevant such as technological and biological applications. In this respect our results can help to build a unified treatment of confined liquids approaching the glass transition having identified some features that are likely general properties of confined liquids such as the enhancement of hopping above T_C.

[1] P. G. Debenedetti, *Metastable Liquids: Concepts and Principles* (Princeton University Press, Princeton, 1997).

[2] *Proceedings of the International Workshop on Dynamics in Confinement*, edited by B. Frick, R. Zorn, and H. Büttner [J. Phys. IV **10**, 3–343 (2000)]; Eur. Phys. J. E **2**, 3–204 (2003), Special Issue for the *International Workshop on Dynamics in Confinement*, edited by B. Frick, M. Koza, and R. Zorn; Eur. Phys. J. Spec. Top. **141**, p. 3–301 (2007), Special Topic for the International Workshop on Dynamics in Confinement, edited by M. Koza, B. Frick, and R. Zorn.

[3] M. Alcoutlabi and G. B. McKenna, J. Phys.: Condens. Matter **17**, R461 (2005).

[4] W. Götze, *Complex Dynamics of Glass Forming Liquids: A Mode Coupling Theory* (Oxford University Press, New York, 2009).

[5] W. Götze and L. Sjögren, Rep. Prog. Phys. **55**, 241 (1992).

[6] W. Götze, *Liquids, Freezing and Glass Transition*, edited by J. P. Hansen, D. Levesque, and J. Zinn-Justin, (North-Holland, Amsterdam, 1991).

[7] W. Götze, J. Phys.: Condens. Matter **11**, A1 (1999).

[8] P. Gallo, M. Rovere, and E. Spohr, Phys. Rev. Lett. **85**, 4317 (2000).

[9] P. Gallo, M. Rovere, and E. Spohr, J. Chem. Phys. **113**, 11324 (2000).

[10] A. Attili, P. Gallo, and M. Rovere, J. Chem. Phys. **123**, 174510 (2005).

[11] P. Gallo, R. Pellarin, and M. Rovere, Europhys. Lett. **57**, 212 (2002).

[12] P. Gallo, R. Pellarin, and M. Rovere, Phys. Rev. E **67**, 041202 (2003).

[13] P. Gallo, R. Pellarin, and M. Rovere, Phys. Rev. E **68**, 061209 (2003).

[14] F. Varnik, J. Baschnagel, and K. Binder, Phys. Rev. E **65**, 021507 (2002).

[15] J. Baschnagel and F. Varnik, J. Phys.: Condens. Matter **17**, R851 (2005).

[16] P. Scheidler, W. Kob, and K. Binder, Europhys. Lett. **52**, 277 (2000).

[17] P. Scheidler, W. Kob, and K. Binder, J. Phys. Chem. B **108**, 6673 (2004).

[18] C. Donati, S. C. Glotzer, P. H. Poole, W. Kob, and S. J. Plimpton, Phys. Rev. E **60**, 3107 (1999).

[19] A. J. Moreno and J. Colmenero, J. Phys.: Condens. Matter **19**, 466112 (2007).

[20] A. J. Moreno and J. Colmenero, Phys. Rev. E **74**, 021409 (2006).

[21] A. J. Moreno and J. Colmenero, J. Chem. Phys. **125**, 164507 (2006).

[22] A. J. Moreno and J. Colmenero, J. Chem. Phys. **123**, 204505 (2005).

[23] V. Krakoviack, Phys. Rev. E **79**, 061501 (2009).

[24] V. Krakoviack, Phys. Rev. E **75**, 031503 (2007).

[25] V. Krakoviack, Phys. Rev. Lett. **94**, 065703 (2005).

[26] V. Krakoviack, J. Phys.: Condens. Matter **17**, S3565 (2005).

[27] J. Kurzidim, D. Coslovich, and G. Kahl, Phys. Rev. Lett. **103**, 138303 (2009).

[28] W. Fenz, I. M. Mryglod, O. Prytula, and R. Folk, Phys. Rev. E **80**, 021202 (2009).

[29] W. Götze and M. Sperl, Phys. Rev. Lett. **92**, 105701 (2004).

[30] W. Götze and M. Sperl, Phys. Rev. E **66**, 011405 (2002).

[31] F. Mallamace, P. Gambadauro, N. Micali, P. Tartaglia, C. Liao, and S.-H. Chen, Phys. Rev. Lett. **84**, 5431 (2000).

[32] F. Sciortino, P. Tartaglia, and E. Zaccarelli, Phys. Rev. Lett. **91**, 268301 (2003).

[33] S. H. Chen, W. R. Chen, and F. Mallamace, Science **300**, 619 (2003).

[34] M. Tokuyama, Physica A **364**, 23 (2006).

[35] M. Tokuyama, Physica A **378**, 157 (2007).

[36] M. Tokuyama, T. Narumi, and E. Kohira, Physica A **385**, 439 (2007).

[37] V. A. Froltsov and S. H. L. Klapp, J. Chem. Phys. **124**, 134701 (2006).
[38] M. L. Rosinberg, in *New Approaches to Problems in Liquid State Theory*, edited by C. Caccamo, J. P. Hansen, and G. Stell (Kluwer Academic Publishers, Dordrecht, NL, 1999).
[39] M. L. Rosinberg, G. Tarjus, and G. Stell, J. Chem. Phys. **100**, 5172 (1994).
[40] L. Sarkisov and P. A. Monson, Phys. Rev. E **61**, 7231 (2000).
[41] K. S. Page and P. A. Monson, Phys. Rev. E **54**, R29 (1996).
[42] W. Kob and H. C. Andersen, Phys. Rev. Lett. **73**, 1376 (1994).
[43] W. Kob and H. C. Andersen, Phys. Rev. E **51**, 4626 (1995).
[44] W. Kob and H. C. Andersen, Phys. Rev. E **52**, 4134 (1995).
[45] S. Sastry, Phys. Rev. Lett. **85**, 590 (2000).
[46] J. Ghosh and R. Faller, J. Chem. Phys. **128**, 124509 (2008).
[47] W. Götze, J. Phys.: Condens. Matter **2**, 8485 (1990).
[48] J. A. Hodgdon and F. H. Stillinger, Phys. Rev. E **48**, 207 (1993).